

Enhancing Strong-Field Dissociation of H_2^+ in Helium Nanodroplets

Lianrong Zhou,¹ Xiaoqing Hu,² Yigeng Peng,³ Junjie Qiang,¹ Peifen Lu,¹ Kang Lin,⁴ Shengzhe Pan,¹
 Xiaochun Gong,¹ Wenyu Jiang,¹ Zhejun Jiang,¹ Chenxu Lu,¹ Hongcheng Ni,¹ Cheng Jin[ⓧ],³ Ruifeng Lu[ⓧ],³
 Yong Wu,^{2,5} Jianguo Wang,² and Jian Wu^{1,6,7,*}

¹State Key Laboratory of Precision Spectroscopy, East China Normal University, Shanghai 200241, China

²Key Laboratory of Computational Physics, Institute of Applied Physics and Computational Mathematics, Beijing 100088, China

³Department of Applied Physics, Nanjing University of Science and Technology, Nanjing 210094, China

⁴Institut für Kernphysik, Goethe-Universität Frankfurt am Main, Frankfurt am Main 60438, Germany

⁵HEDPS, Center of Applied Physics and Technology, Peking University, Beijing 10084, China

⁶Collaborative Innovation Center of Extreme Optics, Shanxi University, Shanxi 030006, China

⁷Chongqing Key Laboratory of Precision Optics, Chongqing Institute of East China Normal University, Chongqing 401121, China



(Received 16 May 2022; accepted 15 December 2022; published 20 January 2023)

We investigate the above-threshold multiphoton ionization of H_2 embedded in superfluid He nanodroplets driven by ultraviolet femtosecond laser pulses. We find that the surrounding He atoms enhance the dissociation of in-droplet H_2^+ from lower vibrational states as compared to that of isolated gas-phase molecules. As a result, the discrete peaks in the photoelectron energy spectrum correlated with the HHe^+ from the dissociative in-droplet molecule shift to higher energies. Based on the electron-nuclear correlation, the photoelectrons with higher energies are correlated to the nuclei of the low-vibrationally excited molecular ion as the nuclei share less photon energy. Our time-dependent nuclear wave packet quantum simulation using a simplified He- H_2^+ system confirms the joint contribution of the driving laser field and the neighboring He atoms to the dissociation dynamics of the solute molecular ion. The results strengthen our understanding of the role of the environment on light-induced ultrafast dynamics of molecules.

DOI: [10.1103/PhysRevLett.130.033201](https://doi.org/10.1103/PhysRevLett.130.033201)

Helium (^4He) nanodroplets with an extremely cold environment at 0.37 K and a broad transparent spectral range are ideal nanoreactors for light-induced physical and chemical reactions of the embedded atoms and molecules [1–3]. The spectroscopy measurements indicate that the in-droplet molecules can rotate freely, manifesting the superfluidity of helium nanodroplets on a microscopic level [4]. This is also visualized in time domain by directly observing the laser-induced rotational alignment dynamics of the in-droplet molecules [5–8]. Moreover, a long-lived coherence in nuclear vibrational dynamics is observed recently in weakly bound In_2 dimers doped in He droplets [9]. As compared to the nuclear motion, the electron acts much faster and thus serves as an ultrafast probe of the condensed environment [10]. Due to the polarization effect of the surrounding He liquid, the ionization potential of the in-droplet molecule is Stark shifted [11]. Depending on the size of the He nanodroplets, the photoelectron spectrum of the in-droplet molecules is observed to shift to higher energy by tens of meV as compared to that of the gas-phase case [11,12]. In the multiphoton region, photoelectron spectra of above-threshold ionization (ATI) of in-droplet atoms or molecules have been recently observed [13–15]. Upon photoionization of molecules, the electronic and nuclear dynamics are activated simultaneously, where the correlation between the electrons and nuclei is expected.

However, most previous works focused on the influence of the surrounding environment on either the nuclear or the electronic dynamics of the in-droplet molecules separately, whereas its effect on the electron-nuclear correlation dynamics remains unrevealed mostly because of the lack of coincidence measurements.

In this Letter, we investigate the multiphoton dissociative ionization of H_2 molecules embedded in superfluid He nanodroplets driven by an intense ultraviolet femtosecond laser pulse. We observed that the discrete peak positions of the ATI photoelectron energy spectrum [16], which are measured in coincidence, shift to higher energies for in-droplet dissociative molecular ions than those of the gas-phase case. Based on the electron-nuclei correlation, the photoionization-created molecular ion launched at low vibrational nuclear states shares less photon energy and thus more energy is deposited into the released photoelectrons. Accordingly, we demonstrate that the He environment enhances the dissociation of the low-vibrationally excited H_2^+ . Our full quantum simulation of dissociation dynamics of a simplified H_2^+ -He system confirms the joint effect of the driving laser field and the neighboring He atoms on the dissociation of low-vibrationally excited states of the in-droplet molecular ions.

Experimentally, the He nanodroplets are produced via the supersonic expansion of pure He gas (>99.9999%)

through a 5- μm -diameter nozzle precooled down to 19 K under 20 bar stagnation pressure. The mean size of generated He nanodroplets is estimated to be ~ 1000 atoms [1,17]. The H_2 molecules in a pickup cell are doped into the He nanodroplet by passing the flying droplet beam through the cell. The gas pressure of the pickup cell is controlled to be $\sim 6 \times 10^{-7}$ mbar so that the nanodroplet has a most likely capture probability of a single H_2 molecule [18]. An ultraviolet femtosecond laser pulse (45 fs, 395 nm) is generated by frequency doubling a near-infrared pulse (40 fs, 790 nm, 10 kHz) in a beta-barium borate (β -BBO) nonlinear crystal and focused onto the He nanodroplets beam in the reaction microscope of a cold target recoil ion momentum spectroscopy (COLTRIMS) setup [19]. The photoelectrons and ions from the in-droplet molecular fragments were detected in coincidence with 0.00008 events per laser shot by two time- and position-sensitive detectors at the opposite ends of the spectrometer. The momentum and kinetic energy of ions and electrons were reconstructed from their time-of-flight (TOF) and positions of impact. The peak intensity of the laser pulses in the interaction zone is estimated to be 5.4×10^{13} W/cm 2 with a Keldysh parameter [20] of 3.1, indicating that multiphoton ionization dominates the ionization process.

Figure 1(a) shows the measured position distribution of ion fragments as a function of TOF, where different ionization channels can be discriminated. The dominating signals are from photoionization created H_2^+ and dissociative product H^+ ions, i.e., $\text{H}_2 + m\hbar\omega \rightarrow \text{H}_2^+ + e(+n\hbar\omega) \rightarrow \text{H} + \text{H}^+ + e$, where m and n are integers of the absorbed photons in the ionization and dissociation steps, respectively [21]. The H_2^+ and H^+ mainly originate from

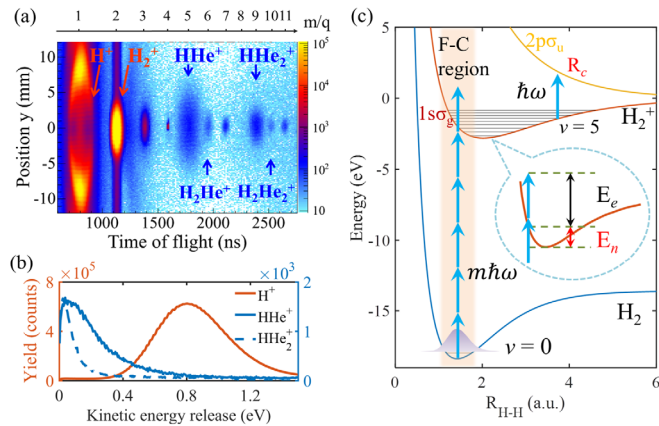


FIG. 1. (a) The yields of ions as a function of their position on the detector along the y axis and their time of flight. The top horizontal axis shows the deduced mass-charge ratio of different ions. (b) The kinetic energy distribution of H^+ , HHe^+ , and HHe_2^+ ions. (c) The potential energy curves of H_2 and H_2^+ . The vertical blue arrows represent the absorption of multiphoton. The inset illustrates the allocation of the remaining photon energy between the nuclei and the electron. The potential energy curve is adapted from [27] and the dissociation limit of $\text{H}^+ + \text{H}$ is set to be zero.

gas-phase H_2 molecules leaked from the pickup cell into the interaction region, which ensures the same laser condition for the measurement as those in-droplet molecules. To unambiguously identify the ionization events from the in-droplet H_2 molecules, we focus on the fragments of HHe^+ and H_2He^+ ions [22–25]. Here the attached He atom serves as a tag, since the surrounding He atoms may influence the light-molecule interaction due to their strong interaction potential and further be attached to the produced ions [26].

For the ATI process investigated here, the absorbed photon energy is shared by the nuclei and electrons of a molecule as a whole [28–32], i.e., $n\hbar\omega = E_e + E_n + I_p + U_p$, where E_e and E_n are the energy deposited into the electrons and nuclei, respectively, I_p is the ionization potential and U_p is the ponderomotive energy of the driving laser field. Because of the mass disparity between the electron and nucleus, the correlation between them is usually ignored in atoms. However, the situation differs for molecules since more degrees of freedom are involved. In particular, the vibrational states serve as the reservoir of the absorbed photon energy. The nuclei of the photoionization-created molecular ion can share more (or less) photon energy by being populated to higher (or lower) vibrational states [28,30]. Figure 1(b) shows the kinetic energy release (KER) distribution for H^+ from gas-phase H_2 molecules and HHe^+ and HHe_2^+ from the in-droplet H_2 molecules. The KER distribution of H^+ is centered at ~ 0.8 eV, which indicates the dissociation of H_2^+ is dominated by the one-photon pathway [33,34], as illustrated in Fig. 1(c). Upon the multiphoton ionization of H_2 , a broad distribution of vibrational states, from $v = 0$ to 10 (peaked at $v = 2$), is prepared in the Franck-Condon region of the electronic ground $1s\sigma_g$ state of H_2^+ . The stretching H_2^+ transits from the $1s\sigma_g$ state to the $2p\sigma_u$ state by absorbing one photon at the internuclear distance of R_c , followed by the dissociation along the $2p\sigma_u$ state. However, for the in-droplet signals of HHe^+ and HHe_2^+ , the KER distributions are substantially altered. Both of them concentrate around ~ 0.1 eV only, which results from the strong interaction of the charged ions with the surrounding He atoms [26]. Therefore, the strong ion-He interaction hinders the straightforward extraction of the original dissociation dynamics of in-droplet molecules from the measured ions of HHe^+ and HHe_2^+ .

According to the electron-nuclear correlation, we can extract the dissociation dynamics of the photoionization-created molecular ion from the ATI spectra of the correlated photoelectrons. Figure 2(a) shows the ATI spectra of the photoelectrons correlated to the H_2^+ and H_2He^+ from gas-phase and in-droplet H_2 molecules respectively. It is surprising that the ATI spectrum of in-droplet H_2He^+ (solid points) shows clear discrete peaks equally spaced by the photon energy similar to that of H_2^+ (circle points).

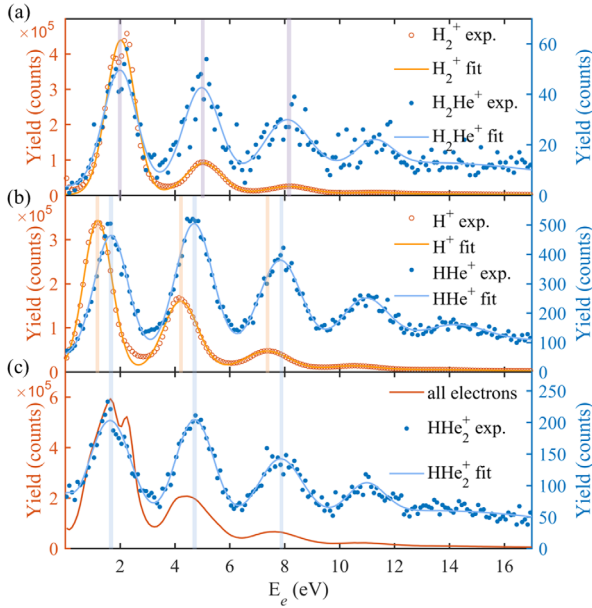


FIG. 2. The measured (circles) energy spectra of photoelectrons correlated with ionic fragments of (a) H_2^+ and H_2He^+ (b) H^+ and HHe^+ , (c) HHe_2^+ and the case of all electrons without coincidence measurements. The vertical lines are used to mark the location of the discrete peaks to guide the eyes. The solid lines are numerical fits to the experimental data with a set of Gaussian functions.

This clearly demonstrates that the dynamics information carried by the kinetic energy of the photoelectrons is preserved. The peak positions of the ATI spectra correlated with the gas-phase H_2^+ and in-droplet H_2He^+ are almost the same, which indicates that the reduction of the ionization potential induced by the polarization effect of the droplet environment can be neglected here. In this Letter, we use He droplets with an average size of ~ 1000 He atoms, which corresponds to a shift of ~ 0.086 eV based on the polarizable continuum model [11,35] and experimental results in Ref. [11]. Hence, the peak positions in the ATI spectrum of H_2He^+ are almost the same as those of H_2^+ .

Interestingly, when looking into the dissociation channels, we find a significant energy shift of ~ 0.5 eV in the discrete peak positions of the ATI spectrum for in-droplet HHe^+ with respect to that for gas-phase H^+ , as shown in Fig. 2(b). Since the reduction of the ionization potential of the in-droplet H_2 is negligible here, the prominent energy shift is attributed to the influence of the surrounding He atoms on the dissociation of the in-droplet H_2^+ . The higher kinetic energy of the photoelectron means that less energy is deposited to the nuclei, indicating the dissociation of in-droplet H_2^+ from a lower vibrational state as compared to that of the gas phase. This photon energy sharing mechanism has been investigated before as a probe of the electron-nuclear dynamics in isolated gas-phase H_2 molecules [29,30]. To reach the critical internuclear distance allowing for the one-photon pathway, the dissociation of

H_2^+ mainly originates from the vibrational states of $v = 5$ in the $1s\sigma_g$ state [33,34]. It is consistent with our experimental results for the gas phased H_2^+ that the total KER of the dissociative product of H^+ and H is ~ 1.6 eV, as shown in Fig. 1(b). Accordingly, the observed ~ 0.5 eV shift to higher energy of the ATI spectrum correlated with HHe^+ indicates that the H_2^+ in vibrational states of $v = 3$ is enhanced to dominate the in-droplet dissociation process. Moreover, as shown in Fig. 2(c), we found that the peak locations of the ATI spectrum correlated with HHe_2^+ are identical to that of HHe^+ , indicating both are from the dissociation of in-droplet H_2^+ of $v = 3$. The ATI spectrum of all electrons without coincidence is plotted in Fig. 2(c), which is dominated by the gas-phase events. We emphasize that coincidence measurement serves as a powerful tool to distinguish in-droplet events from gas-phase events.

To understand the underlying physics, we employ H_2^+ -He as a simplified prototype system to explore the above light-induced dissociation dynamics. Figure 3(a) shows the calculated lowest-lying potential energy surface (PES) of a H_2^+ -He in collinear geometry [26,36,37] as a

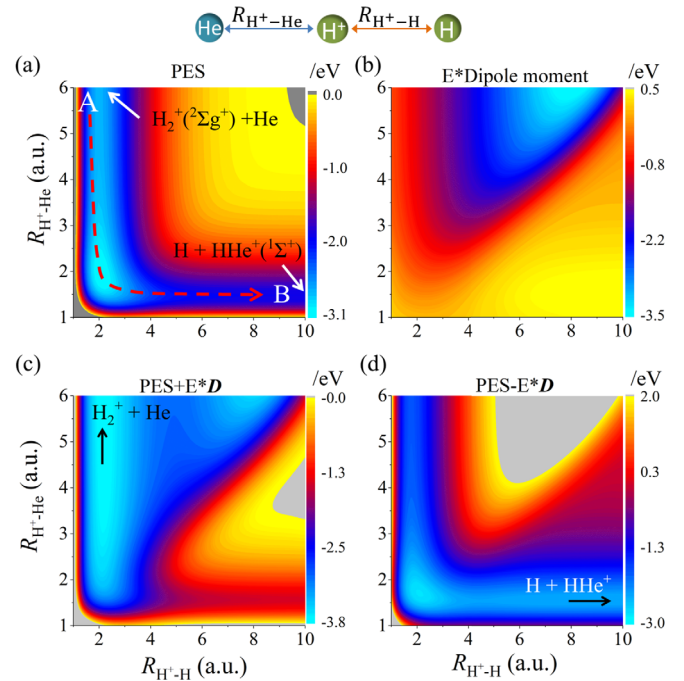


FIG. 3. (a) The calculated lowest-lying adiabatic potential energy surface of the H_2^+ -He as a function of $R_{\text{H}^+-\text{He}}$ and $R_{\text{H}^+-\text{H}}$. The structure of linear H_2^+ -He is depicted at the top. The position of the initial wave packet for H_2^+ -He is labeled by A. The red dashed curve guides the eyes for the wave packet evolution pathway of forming $\text{HHe}^+ + \text{H}$. (b) Potential energy surface of the H_2^+ -He dipole moment in the laser field when the electric field points from He to H_2^+ . Modulated potential energy surfaces by adding $\mathbf{E}(t) * \mathbf{D}$ when the direction of the electric field points (c) from He to H_2^+ and (d) from H_2^+ to He.

function of the internuclear distance $R_{\text{H}^+-\text{H}}$ and $R_{\text{H}^+-\text{He}}$, where $R_{\text{H}^+-\text{H}}$ and $R_{\text{H}^+-\text{He}}$ are the internuclear distance between the centered H^+ with H and He, respectively. In our *ab initio* calculations, the combined MCSCF + ic-MRCI method implemented in the MOLPRO package [38–40] and the d-aug-cc-pVQZ basis set were employed. As shown in Fig. 3(a), the PES of the ground state of the linear H_2^+-He complex has minimal energy at the equilibrium internuclear distances of $R_{\text{H}^+-\text{H}} = 2.1$ and $R_{\text{H}^+-\text{He}} = 1.9$ a.u.. Since the system starts from a neutral H_2 molecule doped inside the He droplet and the instant photoionization does not change the internuclear distance, the initial nuclear wave packet of H_2^+-He can be obtained by projecting the Gaussian wave packet centered at the equilibrium structure of H_2-He according to the Frank-Condon principle, labeled by the A in Fig. 3(a). The ground state of $\text{H} + \text{HHe}^+(\ ^1\Sigma^+)$ product (-2.0 eV), where $R_{\text{H}^+-\text{H}} = \infty$, $R_{\text{H}^+-\text{He}} = 1.5$ a.u., lies 0.8 eV above that of $\text{H}_2^+(\ ^2\Sigma_g^+) + \text{He}$ (-2.8 eV), where $R_{\text{H}^+-\text{H}} = 2.0$ a.u., $R_{\text{H}^+-\text{He}} = \infty$. Because of the energy barrier, the vibrationally excited H_2^+ with $v \geq 3$ can lead to the formation of $\text{H} + \text{HHe}^+$ under the field-free condition. The possible evolution path of the nuclear wave packet is guided by the red dashed curve with an arrow from A to B in Fig. 3(a) [also see Figs. 4(a1)–4(a4)]. For the dissociation of isolated gas-phase H_2^+ , the generation of H^+ is dominant by vibrationally excited H_2^+ with $v = 5$. In contrast, we find that the H_2^+ populating on $v = 3$ in H_2^+-He has a certain possibility to produce HHe^+ , which accounts for the observed energy shift of the discrete peaks of the ATI spectrum correlated with the HHe^+ as compared to the one of H^+ .

In the following, we further investigate the laser-induced dissociation dynamics of H_2^+ in H_2^+-He . Since the laser field will last for a period after the ionization around the pulse peak, the dipole interaction of $\mathbf{E}(t) * \mathbf{D}$ between the laser field and the molecular ion H_2^+-He is considered, where $\mathbf{E}(t)$ is the electric field of laser pulses and \mathbf{D} is the dipole moment of H_2^+-He . As shown in Fig. 3(b), the peak

magnitude of $\mathbf{E}(t) * \mathbf{D}$ is comparable to the potential energy of H_2^+-He . As a result, with the electric field pointing from He to H_2^+ , as shown in Fig. 3(c), the H_2^+-He system is favored to dissociate into $\text{H}_2^+ + \text{He}$. Whereas, with the opposite direction of the electric field, the formation of $\text{H} + \text{HHe}^+$ is preferable, since it becomes barrierless along the PES, as guided by the black arrow in Fig. 3(d).

To visualize the intrinsic dynamics mechanism, we performed a full quantum time-dependent wave packet simulation to study the laser-driven dissociation processes of H_2^+-He [41]. The proportion of the $\text{H} + \text{HHe}^+$ channel can be obtained under different initial conditions with H_2^+ populating on $v = 0, 1, 2, \dots$ (see more theoretical details in the Supplemental Material [42]). Here, we focus on the vibrational state of $v = 3$ as it governs the dissociation process of the in-droplet molecules. Starting from the equilibrium internuclear distance of neutral H_2-He , the evolution of the nuclear wave packet for H_2^+-He under the field-free condition is shown in Figs. 4(a1)–4(a4). The probability of producing $\text{H} + \text{HHe}^+$ channel is only $\sim 3.25\%$ without the action of laser pulses, since the energy stored in the H–H stretching mode is barely enough to overcome the energy barrier of 0.8 eV between $\text{H}_2^+(\ ^2\Sigma_g^+) + \text{He}$ and $\text{H} + \text{HHe}^+(\ ^1\Sigma^+)$ product. Interestingly, after taking the dipole interaction into consideration, the probability to produce $\text{H} + \text{HHe}^+$ increases to 13.03% , as shown in Figs. 4(b1)–4(b4). To this end, we demonstrate that the vibrationally excited states with $v = 3$ of H_2^+ in He droplet is enhanced to dissociate, which agrees quantitatively with the experimentally observed energy shift of the ATI spectrum correlated with HHe^+ .

In summary, we have investigated the strong-field multi-photon dissociative ionization of H_2 molecules embedded in He nanodroplets. We identified the ATI spectra of photoelectrons correlated with specific reaction channels of the in-droplet and gas-phase H_2 molecules by coincidence measurement. In contrast to H^+ from the dissociative

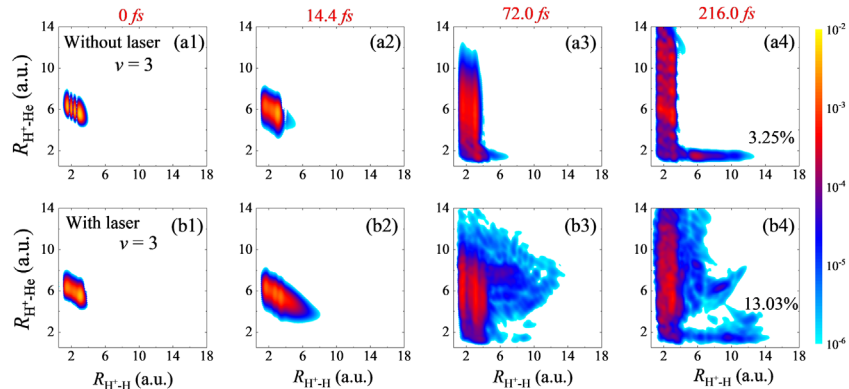


FIG. 4. (a1)–(a4) Field-free and (b1)–(b4) laser-driven dissociation dynamics of H_2^+-He nuclear wave packet for vibrational state $v = 3$ at different times.

ionization of gas-phase H_2 , an energy shift of 0.5 eV to higher values in ATI spectrum correlated with the HHe^+ ion is observed, which is attributed to the enhanced dissociation of in-droplet H_2^+ from the low vibrational states. This intuitive scenario is confirmed by full quantum time-dependent nuclear wavepacket simulations of a simplified H_2^+ -He model system. Our results pave the way towards understanding and further steering the light-induced electron-nuclear correlation dynamics in He nanodroplets.

This work is supported by the National Key R&D Program of China (Grant No. 2018YFA0306303); the National Natural Science Fund (Grants No. 11834004, No. 12227807, No. 11621404, No. 12174109, No. 92050105, No. 11934004, No. 12104063, and No. 12241407).

L. Zhou and X. Hu contributed equally to this work.

*jwu@phy.ecnu.edu.cn

- [1] J. P. Toennies and A. F. Vilesov, Superfluid helium droplets: A uniquely cold nanomatrix for molecules and molecular complexes, *Angew. Chem., Int. Ed.* **43**, 2622 (2004).
- [2] M. P. Ziemkiewicz, D. M. Neumark, and O. Gessner, Ultrafast electronic dynamics in helium nanodroplets, *Int. Rev. Phys. Chem.* **34**, 239 (2015).
- [3] S. Albertini, E. Gruber, F. Zappa, S. Krasnokutski, F. Laimer, and P. Scheier, Chemistry and physics of dopants embedded in helium droplets, *Mass Spectrom. Rev.* **41**, 529 (2021).
- [4] M. Hartmann, R. E. Miller, J. P. Toennies, and A. Vilesov, Rotationally Resolved Spectroscopy of SF_6 in Liquid Helium Clusters: A Molecular Probe of Cluster Temperature, *Phys. Rev. Lett.* **75**, 1566 (1995).
- [5] D. Pentleher, J. H. Nielsen, A. Slenczka, K. Molmer, and H. Stapelfeldt, Impulsive Laser Induced Alignment of Molecules Dissolved in Helium Nanodroplets, *Phys. Rev. Lett.* **110**, 093002 (2013).
- [6] A. S. Chatterley, C. Schouder, L. Christiansen, B. Shepperson, M. H. Rasmussen, and H. Stapelfeldt, Long-lasting field-free alignment of large molecules inside helium nanodroplets, *Nat. Commun.* **10**, 133 (2019).
- [7] A. S. Chatterley, L. Christiansen, C. A. Schouder, A. V. Jørgensen, B. Shepperson, I. N. Cherepanov, G. Bighin, R. E. Zillich, M. Lemeshko, and H. Stapelfeldt, Rotational Coherence Spectroscopy of Molecules in Helium Nanodroplets: Reconciling the Time and the Frequency Domains, *Phys. Rev. Lett.* **125**, 013001 (2020).
- [8] J. Qiang, L. Zhou, P. Lu *et al.*, Femtosecond Rotational Dynamics of D_2 Molecules in Superfluid Helium Nanodroplets, *Phys. Rev. Lett.* **128**, 243201 (2022).
- [9] B. Thaler, M. Meyer, P. Heim, and M. Koch, Long-Lived Nuclear Coherences inside Helium Nanodroplets, *Phys. Rev. Lett.* **124**, 115301 (2020).
- [10] B. Thaler, S. Ranftl, P. Heim, S. Cesnik, L. Treiber, R. Meyer, A. W. Hauser, W. E. Ernst, and M. Koch, Femtosecond photoexcitation dynamics inside a quantum solvent, *Nat. Commun.* **9**, 4006 (2018).
- [11] E. Loginov, D. Rossi, and M. Drabbels, Photoelectron Spectroscopy of Doped Helium Nanodroplets, *Phys. Rev. Lett.* **95**, 163401 (2005).
- [12] M. Mudrich and F. Stienkemeier, Photoionisation of pure and doped helium nanodroplets, *Int. Rev. Phys. Chem.* **33**, 301 (2014).
- [13] L. Treiber, B. Thaler, P. Heim, M. Stadlhofer, R. Kanya, M. Kitzler-Zeiler, and M. Koch, Observation of laser-assisted electron scattering in superfluid helium, *Nat. Commun.* **12**, 4204 (2021).
- [14] M. Kelbg, M. Zabel, B. Krebs, L. Kazak, K. H. Meiwes-Broer, and J. Tiggesbaumer, Temporal Development of a Laser-Induced Helium Nanoplasma Measured through Auger Emission and Above-Threshold Ionization, *Phys. Rev. Lett.* **125**, 093202 (2020).
- [15] R. Michiels, M. Abu-Samha, L. B. Madsen *et al.*, Enhancement of Above Threshold Ionization in Resonantly Excited Helium Nanodroplets, *Phys. Rev. Lett.* **127**, 093201 (2021).
- [16] P. Agostini, F. Fabre, G. Mainfray, G. Petite, and N. K. Rahman, Free-Free Transitions Following Six-Photon Ionization of Xenon Atoms, *Phys. Rev. Lett.* **42**, 1127 (1979).
- [17] M. Y. Choi, G. E. Douberly, T. M. Falconer, W. K. Lewis, C. M. Lindsay, J. M. Merritt, P. L. Stiles, and R. E. Miller, Infrared spectroscopy of helium nanodroplets: novel methods for physics and chemistry, *Int. Rev. Phys. Chem.* **25**, 15 (2006).
- [18] M. Lewerenz, B. Schilling, and J. P. Toennies, Successive capture and coagulation of atoms and molecules to small clusters in large liquid helium clusters, *J. Chem. Phys.* **102**, 8191 (1995).
- [19] R. Dörner, V. Mergel, O. Jagutzki, L. Spielberger, J. Ullrich, R. Moshhammer, and H. Schmidt-Böcking, Cold Target Recoil Ion Momentum Spectroscopy: A 'momentum microscope' to view atomic collision dynamics, *Phys. Rep.* **330**, 95 (2000).
- [20] L. V. Keldysh, *Zh. Eksp. Teor. Fiz.* **47**, 1945 (1964).
- [21] J. H. Posthumus, The dynamics of small molecules in intense laser fields, *Rep. Prog. Phys.* **67**, 623 (2004).
- [22] T. M. Kojima, N. Kobayashi, and Y. Kaneko, Formation of helium cluster ions HHe_x^+ ($x \leq 14$) and $H_3He_x^+$ ($x \leq 13$) in a very low temperature drift tube, *Z. Phys. D* **23**, 181 (1992).
- [23] M. Fárník and J. P. Toennies, Ion-molecule reactions in 4He droplets: Flying nano-cryo-reactors, *J. Chem. Phys.* **122**, 014307 (2005).
- [24] P. Bartl, C. Leidlmair, S. Denifl, P. Scheier, and O. Echt, Cationic complexes of hydrogen with helium, *ChemPhysChem* **14**, 227 (2013).
- [25] L. Lundberg, P. Bartl, C. Leidlmair, P. Scheier, and M. Gatchell, Protonated and cationic helium clusters, *Molecules* **25**, 1066 (2020).
- [26] M. Meuwly and J. M. Hutson, The potential energy surface and near-dissociation states of $He-H_2^+$, *J. Chem. Phys.* **110**, 3418 (1999).
- [27] T. E. Sharp, Potential-energy curves for molecular hydrogen and its ions, *At. Data Nucl. Data Tables* **2**, 119 (1970).
- [28] R. E. F. Silva, F. Catoire, P. Rivière, H. Bachau, and F. Martín, Correlated Electron and Nuclear Dynamics in Strong Field Photoionization of H_2^+ , *Phys. Rev. Lett.* **110**, 113001 (2013).

- [29] C. B. Madsen, F. Anis, L. B. Madsen, and B. D. Esry, Multiphoton Above Threshold Effects in Strong-Field Fragmentation, *Phys. Rev. Lett.* **109**, 163003 (2012).
- [30] J. Wu, M. Kunitski, M. Pitzer *et al.*, Electron-Nuclear Energy Sharing in Above-Threshold Multiphoton Dissociative Ionization of H_2 , *Phys. Rev. Lett.* **111**, 023002 (2013).
- [31] P. Lu, J. Wang, H. Li *et al.*, High-order above-threshold dissociation of molecules, *Proc. Natl. Acad. Sci. U.S.A.* **115**, 2049 (2018).
- [32] W. Zhang, P. Lu, J. Ma, H. Li, X. Gong, and J. Wu, Correlated electron–nuclear dynamics of molecules in strong laser fields, *J. Phys. B* **53**, 162001 (2020).
- [33] K. Sändig, H. Figger, and T. W. Hänsch, Dissociation Dynamics of H_2^+ in Intense Laser Fields: Investigation of Photofragments from Single Vibrational Levels, *Phys. Rev. Lett.* **85**, 4876 (2000).
- [34] J. McKenna, F. Anis, B. Gaire, N. G. Johnson, M. Zohrabi, K. D. Carnes, B. D. Esry, and I. Ben-Itzhak, Suppressed Dissociation of H_2^+ Vibrational States by Reduced Dipole Coupling, *Phys. Rev. Lett.* **103**, 103006 (2009).
- [35] J. Jortner, Cluster size effects, *Z. Phys. D* **24**, 247 (1992).
- [36] T. Szidarovszky and K. Yamanouchi, Photodissociation dynamics of weakly bound HeH_2^+ in intense light fields, *Phys. Rev. A* **94**, 063405 (2016).
- [37] P. Palmieri, C. Puzzarini, V. Aquilanti, G. Capecchi, S. Cavalli, D. De Fazio, A. Aguilar, X. Giménez, and J. M. Lucas, Ab initio dynamics of the $He + H_2^+ \rightarrow HeH^+ + H$ reaction: a new potential energy surface and quantum mechanical cross-sections, *Mol. Phys.* **98**, 1835 (2000).
- [38] H. J. Werner, P. J. Knowles, G. Knizia, F. R. Manby, and M. Schütz, Molpro: a general-purpose quantum chemistry program package, *Comput. Mol. Sci.* **2**, 242 (2012).
- [39] H. J. Werner, P. J. Knowles, F. R. Manby *et al.*, The Molpro quantum chemistry package, *J. Chem. Phys.* **152**, 144107 (2020).
- [40] H. J. Werner, P. J. Knowles, G. Knizia *et al.*, MOLPRO 2019, a package of ab initio programs, see <https://www.molpro.net>.
- [41] X. Hu, C. Jia, T. Xu, Y. Wu, and J. Wang, Full quantum time-dependent simulations for the two-body breakups of H_2Ar^{2+} and N_2Ar^{2+} , *Phys. Rev. A* **106**, 012814 (2022).
- [42] See Supplemental Material at <http://link.aps.org/supplemental/10.1103/PhysRevLett.130.033201> for full quantum time-dependent wave packet evolution method.